Journal of Futuristic Sciences and Applications
Vol. 7(2), Jul-Dec 2024, pp. 15-40
doi: 10.51976/jfsa.722403
www.gla.ac.in/journals/jfsa
© 2024 JFSA, GLA University

A Systematic Review of Propeller Design and Optimization in Low-Reynolds Regime Unmanned Aerial Vehicles(UAV)

Aditya Garg, Abhinna Kumar Sahoo**, Aditya Nirwal*** and Pulijala Pawan Kumar*****

ABSTRACT

Low Reynolds Number aerodynamics in Unmanned Aerial Vehicles (UAVs) and micro-UAVs (MUAVs) present critical challenges, including early flow separation, reduced propulsive efficiency, and high sensitivity to geometric conditions. This review highlights the foundational principles of airfoil theory, lift generation and pressure distribution. This extends to rotating propeller system, covering momentum theory, Blade Element Theory (BET), and Blade Element Momentum Theory (BEMT). The analysis examines geometric design variables, airfoil selection strategies and the different constraints of structural mechanics and aeroacoustics. Key findings identify specialized low-Re airfoils as essential for managing laminar separation bubbles where conventional models fail. Furthermore, a strong electromechanical coupling between propeller performance and motor–battery dynamics is identified as a major contributing factor to system efficiency. This work establishes a unified framework for the integrated design and optimization of high-performance UAV propulsion systems.

Keywords: *Low Reynolds number aerodynamics; Laminar separation bubbles; BEMT; Aeroacoustics.*

1.0 Introduction

Unmanned aerial vehicles (UAVs), particularly micro and small UAV (MUAV) platforms, have become essential across the aerospace and defense industries and in environmental monitoring. Advances in lightweight structures, electric propulsion and computational aerodynamics have enabled access to challenging environments. However, due to Low-Reynolds-number aerodynamics, propulsive inefficiencies and system integration challenges are faced. The core of UAV performance is the propeller system, which converts rotational power to thrust. Unlike fixed-wings, propeller blades face non-uniform inflows with variations in Reynolds number, Mach number and velocities. This combines aerodynamics, structural research and acoustics, transforming design into an optimization task. A key challenge arises in Low-Reynolds-number regimes, where boundary layers respond sharply to surface roughness, laminar separation bubbles and early transition.

**Corresponding author; Researcher Scholar, Department of Mechanical Engineering, Delhi Technological University, New Delhi, Delhi, India (E-mail: adityagarg2109@gmail.com)*
***Researcher Scholar, Department of Mechanical Engineering, Delhi Technological University, New Delhi, Delhi, India (E-mail: abhinna.chintu@gmail.com)*
****Researcher Scholar, Department of Mechanical Engineering, Delhi Technological University, New Delhi, Delhi, India (E-mail: nirwaladitya7@gmail.com)*
*****Researcher Scholar, Department of Mechanical Engineering, Delhi Technological University, New Delhi, Delhi, India (E-mail: songsoffire1997@gmail.com)*

Doi: 10.51976/jfsa.722403

Conventional airfoils fail here, requiring specialized low-Re designs and advanced computational predictions of lift, drag and stall. Often overlooked is the direct impact on system-level constraints. Designs for Battery energy density, motor efficiency profiles and electronic speed controllers fall short. An integrated aerodynamic framework is essential. In the past decade, scientists have progressed in airfoil theory, propeller models and optimization methods. However, a unified thinking of airfoil physics, propeller performance and UAV integration remains scarce, especially amidst the rising demand from micro aerial vehicles, urban air mobility and bio-inspired designs that give huge importance to efficiency, noise and endurance.

2.0 Airfoils: Foundation and Low-Reynolds Aerodynamics

2.1 Physics and force generation

The development of the airfoil section represents a critical advancement in fluid mechanics and aerospace engineering [1], where an airfoil is a shaped surface designed to modify airflow and generate aerodynamic forces essential for lift production .In modern times, understanding of airfoil theory has evolved from early observations inspired by bird wings to a more research-rigorous and physics-based framework [2].

To build this foundation, we begin with the fundamental mechanisms of lift generation. The Bernoulli principle and the conservation of momentum are collectively used for the generation of lift. When a fluid encounters an airfoil, the geometry and angle of attack force the streamlines to contract over the upper surface, which results in an increase in local velocity. The incompressible Bernoulli equation is given by [3]:

$$P + \frac{1}{2}\rho V^2 = C \quad \ldots(1)$$

According to this framework, increase in velocity (V) leads to a decrease in static pressure (P) on the suction side, creating a pressure difference that contributes to the upward lift force on the wing. Simultaneously, the conservation of momentum—derived from Newton's third law—demands that the airfoil deflect the air downward. The downward momentum imparted to the fluid results in an equal and opposite upward reaction force [2].

Table 1: Various Aerodynamic Force Components

Component	Physical Source	Orientation	Effect on Performance
Lift (L)	Pressure differential	Normal to freestream	Primary useful force for flight
Drag (D)	Pressure imbalance & Shear	Parallel to freestream	Resistance to motion, requires thrust
Pitching Moment (M)	Asymmetric pressure	Torque about reference	Affects longitudinal stability
Skin Friction	Viscous shear stress	Tangential to surface	Major drag component at high Re

2.2 Pressure distribution and aerodynamic center

To effectively scale wind tunnel data to real-world UAV applications, non-dimensional variables are required. The Pressure Coefficient (C_p) serves as the primary tool for identifying nature of flow [4]. By normalizing local static pressure relative to the freestream, C_p maps the aerodynamic "work" being done by the surface [5]. The Pressure Coefficient is defined as:

$$C_p = \frac{p - p_\infty}{q_\infty} \quad \ldots(2)$$

A sharp leading-edge suction peak indicates high-lift conditions but also signals potential separation risk [6]. On the other hand, trailing-edge pressure recovery determines boundary layer stability under adverse pressure gradients [7]. In design, we must distinguish between the "Center of Pressure" and the "Aerodynamic Center" (AC). While the Center of Pressure is the point where the net pressure force acts, it shifts as the angle of attack changes, complicating the longitudinal balance [8]. Conversely, the AC is the point where the pitching moment remains nearly constant [5].

The Pitching Moment Coefficient (C_m) quantifies the characteristic behavior of an airfoil's torque and is defined as:

$$C_m = \frac{M}{q_\infty S_c} \quad ...(3)$$

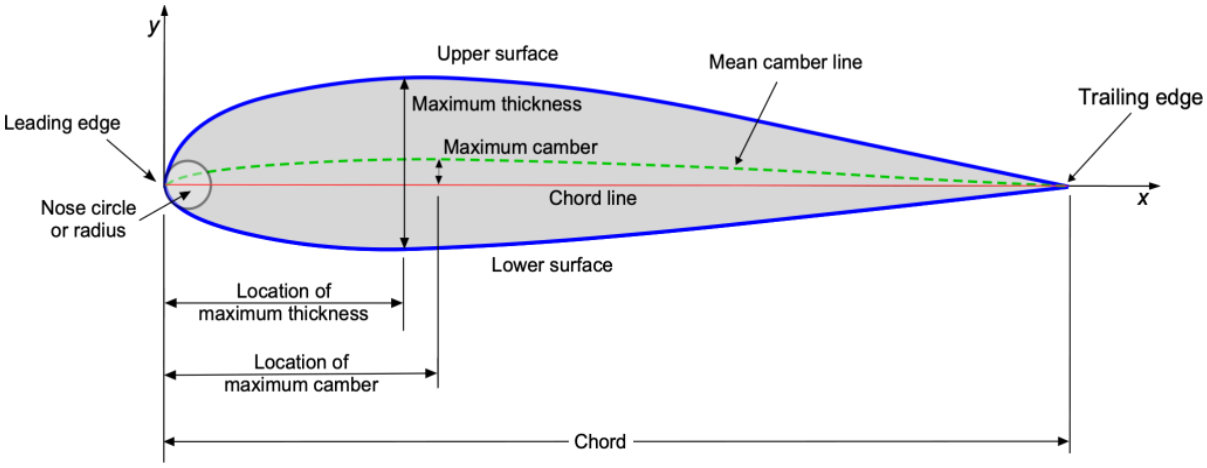
Explicitly, for the vast majority of subsonic airfoils, the "quarter-chord" rule applies, placing the AC at approximately 25% of the chord length from the leading edge [8]. Conventional airfoils with positive camber typically exhibit a negative, nose-down pitching moment about this point, which demands counterbalancing forces from the tail to maintain trim [5]. Airfoil geometry fundamentally governs these pressure-based aerodynamic characteristics and serves as the primary design variable influencing lift generation and flow behavior.

2.3 Geometric parametrization and performance trade-offs

Modern parametrization relies on the relationship between the chord line, the mean camber line and the thickness distribution. The chord line is the straight reference connecting the leading and trailing edges, while the mean camber line is the locus of points equidistant from the upper and lower surfaces[9]. Critically, increasing the maximum camber "shifts the lift-curve" upward, allowing for lift generation at zero angle of attack [9].

However, this increase in camber introduces a stronger nose-down pitching moment, requiring larger stabilizing surfaces and increasing trim drag. Airfoil design typically involves balancing several competing requirements between lift, drag and structural volume. Thick airfoils provide necessary internal volume for spars and fuel and they often provide a "softer" stall because the rounded nose allows the flow to remain attached at higher angles of attack [10]. However, increasing thickness accelerates local flow to supersonic speeds even when the aircraft is subsonic, causing the airfoil to reach its Critical Mach Number (M_{crit}) prematurely[9].

Figure 1: The Key Geometric Parameters that Define the Shape of an Airfoil [9]



Doi: 10.51976/jfsa.722403

Table 2: Influence of Airfoil Geometric Parameters on Aerodynamic Performance Metrics (Lift, Drag and Critical Mach Number)

Geometric Parameter	Change	Effect on $C_{l,\,max}$	Effect on $C_{d,\,min}$	Effect on M_{crit}
Max Camber	Increase	Increase	Increase	Decrease
Max Thickness	Increase	Increase (to ~12%)	Increase	Decrease
Thickness Position	Move Aft	Decrease	Decrease	Increase
LE Radius	Increase	Increase	Increase	Decrease

2.4 Reynolds and mach regime

The concept of flow similarity is the cornerstone of experimental aerodynamics, allowing engineers to apply wind tunnel data to full-scale vehicles. While the Mach number governs compressibility [11], the Reynolds number (Re) is the dominant variable for small-scale UAVs [12]. Formula for Re is:

$$Re = \frac{\rho V c}{\mu} \quad ...(4)$$

At the "Viscous Scale" typical of small UAVs (often between 10,000 and 200,000), boundary layers are thick and highly prone to separation [13]. A critical transition occurs at Re = 70,000, where airfoils often experience a dramatic jump in efficiency as the flow gains sufficient energy to reattach after initial separation [14]. Above Re = 1,000,000, the flow is predominantly turbulent, characterized by thinner boundary layers that allow for higher lift-to-drag ratios common in commercial aviation[13].

Contrastingly, the Mach number (M) defines how the fluid responds to pressure changes. In the subsonic regime ($M < 0.3$), air is treated as incompressible [1]. As speeds increase into the transonic regime ($0.7 < M < 1.2$), local velocities on the upper surface may exceed the speed of sound, creating shock waves that interact with the boundary layer [1]. In the supersonic regime ($M > 1.2$), the entire flow field is faster than the speed of sound and lift is generated via compression and expansion waves [1].

2.5 Low-Reynolds aerodynamics and laminar separation bubbles

Micro Air Vehicles (MAVs) operating between Re 10,000 and 200,000 exist in a unique and unforgiving aerodynamic environment. In this regime, the flow is almost entirely laminar and exceptionally sensitive to adverse pressure gradients. This sensitivity leads to the formation of the Laminar Separation Bubble (LSB). A laminar separation bubble forms when the boundary layer detaches [14], transitions to turbulence and reattaches downstream [15].

The impact of "bubble bursting" is catastrophic. If the flow fails to reattach, it results in premature stall and a massive loss of efficiency [7]. To manage these viscous challenges, specialized airfoils like the MH32 and SD7032 employ "transition ramps" [16]. These ramps are subtle geometric features designed to force a controlled transition and reattachment of the LSB, maintaining aerodynamic health at ultra-low speeds [15].

2.6 Evolution: From NACA to XFOIL

The shift from empirical "cut-and-try" methods to systematic computational synthesis was pioneered by the National Advisory Committee for Aeronautics (NACA). The NACA 4-digit series was the first family defined mathematically: the first digit indicates max camber (percent chord), the second indicates the location of max camber (tenths of chord) and the last two indicate max thickness

(percent chord)[17]. The 5-digit series moved camber forward for higher lift, while the 6-series utilized "inverse design" to specify a desired pressure distribution intended to maintain laminar flow [18]. A revolutionary breakthrough was XFOIL, developed by Mark Drela at MIT in 1989 [19]. XFOIL enabled the coupling of panel methods with integral boundary layer models for accurate prediction of low-Reynolds-number separation phenomena [20].

Concurrent with this was Richard Whitcomb's development of the Supercritical airfoil, which used a flatter upper surface to delay wave drag. Whitcomb's "coved" trailing edge allows for higher cruise speeds by pushing the shock wave further aft and weakening its intensity. These developments converge in the design of modern, highly specialized UAV propellers. Figure 2 shows the comparison of conventional and supercritical airfoils[21].

Figure 2: Comparison of Conventional and Supercritical Airfoils [21]

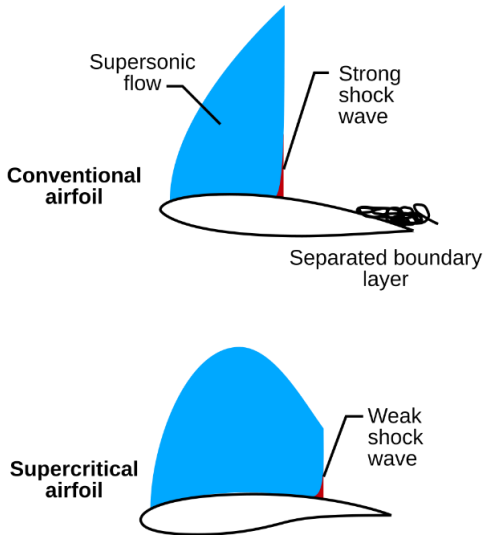


Table 3: Comparative Aerodynamic Characteristics of Conventional and Supercritical Airfoil Designs

Feature	Conventional Airfoil	Supercritical Airfoil
Upper Surface	Highly curved	Relatively flat
Leading Edge	Smaller radius	Large, blunt radius
Trailing Edge	Straight	"Cove" or aft-loaded
Shock Location	Forward/Strong	Aft/Weaker
Benefit	Good low-speed lift	Higher cruise Mach number

2.7 Application to propeller-focused UAV design

These principles directly extend to rotating propeller blades which requires synthesizing requirements for sections that handle varying Re and Mach numbers from hub to tip. For UAVs, the selection of airfoil sections like the MH32 is not merely a preference but a requirement for battery life and payload capacity. The MH32's ability to manage LSBs directly impacts the thrust-to-power ratio of the vehicle [16]. Efficient sections at the propeller tip, where Re is higher but Mach numbers approach transonic limits, are essential for modern MAV performance[22].

Doi: 10.51976/jfsa.722403

3.0 Propeller Aerodynamics and Design

3.1 Strategic role of propeller propulsion

The strategic landscape of modern aviation is undergoing a paradigm shift driven by Unmanned Aerial Vehicles (UAVs) and Urban Air Mobility (UAM). Propeller engineering has evolved from early theoretical skepticism into a multidisciplinary field integrating fluid mechanics, structural dynamics and computational optimization [23]. Modern systems must satisfy stringent performance and acoustic requirements, particularly in distributed electric propulsion (DEP) architectures [24].

Propellers are structures that extend 2D airfoil theory into a rotating 3D system. Unlike fixed wings, propeller blades operate in a radially varying velocity field combining axial velocity $V_{forward}$ and tangential velocity $V_{rot} = \Omega r$ [25]. This necessitates a transition from lift-based analysis to momentum-based modeling.

3.2 Momentum theory and the actuator disk model

Momentum Theory (Actuator Disk Theory) provides a first-order estimate of propeller performance by modeling the propeller as an energy-converting disk [26].

The actuator disk introduces a pressure jump Δp, accelerating the flow from freestream velocity V_∞ to wake velocity V_e .

Applying Bernoulli's equation upstream and downstream yields:

$$\Delta p = \frac{1}{2}\rho(V_e^2 - V_\infty^2) \quad ...(5)$$

Thrust is expressed as:

$$T = \rho A V d(V_e - V_\infty) \quad ...(6)$$

Equating pressure-based and momentum-based expressions gives the key relation:

$$V_d = \frac{1}{2}(V_\infty + V_e) \quad ...(7)$$

The Betz Limit defines the maximum theoretical efficiency:

$$C_p^{max} = \frac{16}{27} \approx 0.593 \quad ...(8)$$

3.3 Blade Element Theory (BET) and force resolution

Blade Element Theory (BET) refines analysis by dividing the blade into radial elements and applying 2D airfoil data locally [27].

For a blade element located at radius r, the local flow is characterized by the inflow angle ϕ, defined as the angle between the relative wind velocity and the plane of rotation. The aerodynamic forces acting on the element consist of lift dL (perpendicular to the relative wind) and drag dD (parallel to the relative wind) [28].

For an element at radius r:

$$dT = dL\cos\phi - dD\sin\phi \quad ...(9)$$

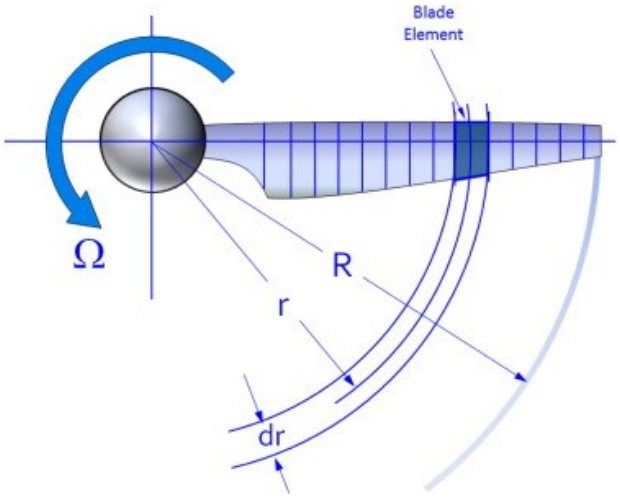
$$dQ = (dL\sin\phi + dD\cos\phi)r \quad ...(10)$$

The blade pitch angle θ, defined as the angle between the blade chord and the plane of rotation, is related to the inflow angle ϕ through the angle of attack α :

$$\alpha = \theta - \phi \quad ...(11)$$

Accuracy of this theory depends heavily on sectional airfoil data (C_l, C_d), often obtained from NACA databases or XFOIL simulations [29].

Figure 3: Schematic of a Propeller of Radius R Rotating with Angular Velocity Ω. A Representative Blade Element is Shown with Chord Length c(r), Width dr, and Centerline Located at Radial Position r [27]



3.4 Unified modeling: Blade Element Momentum Theory (BEMT) and CFD paradigms

Blade Element Momentum Theory (BEMT) combines Momentum Theory and Blade Element Theory (BET) by solving for axial and tangential induction factors (a, a′), allowing it to account for wake rotation effects [26]. It remains the industry standard for UAV propeller design as it strikes a good balance between accuracy and computational efficiency [27]. Important refinements to the method include the Prandtl tip loss factor for finite blade effects [29] and reformulated BEMT that improve performance under low-inflow conditions typical of UAM systems [27]. Beyond BEMT, higher-fidelity approaches are also used such as MRF methods for steady-state CFD, Sliding Mesh techniques for unsteady CFD and Vortex-Based Methods (VBM) for system-level analyses.

3.5 Geometric architecture

Geometric selection—diameter, pitch and chord—serves as the primary driver of mission capability and the acoustic footprint.

3.5.1 Diameter scaling and optimization

The tip diameter (D) is the dominant scaling parameter, with thrust scaling as D^4 and power/torque scaling as D^5[30]. Large-diameter propellers move more air at lower velocities, improving static thrust, but are constrained by tip Mach number limits to avoid compressibility losses [23]. Modern optimization utilizes Parametric Modeling with Bezier curves to define chord and twist distributions [31].

3.5.2 Pitch, slip and altitude twist

In real operation, effective pitch is lower than geometric pitch due to slip. Blade "Twist" ensures optimal angles of attack across varying tangential velocities [25]. This is strategically varied based on mission altitude: high-altitude designs often utilize a 25° twist compared to 15° for low-altitude variants to compensate for reduced air density [32].

Doi: 10.51976/jfsa.722403

3.6 Airfoil selection in low reynolds number regimes

At extremely low Re, thin cambered plates often outperform thicker sections by maintaining attached flow and high L/D ratios [33].

Table 4: Comparative Analysis of Airfoil Geometries for Different UAVs

Airfoil Type	Typical Application	Key Characteristics
Clark-Y	Small UAVs	Flat bottom, robust $C_{l,max}$ at $Re \approx 75{,}000$ [34], [35].
NACA 0012	General Aviation	Symmetrical, extensively documented [33].
Thin Plates	Micro UAVs (MAVs)	Superior lift/drag below $Re = 50{,}000$ [9].
SD8020	UAV Tail/Rudders	High stability and pitch control [34] .
Scimitar	High-Performance UAV	Swept-tip design for drag reduction and acceleration [36].

3.7 Structural mechanics: Materials, fatigue and dynamic stability

Structural integrity must balance stiffness against centrifugal loads that can exceed thousands of Gs.

3.7.1 Material selection: CFRP vs. Metal

Professional UAVs prioritize Carbon Fiber Reinforced Polymers (CFRP) due to their superior strength-to-weight ratios. Unlike the linear fatigue of metals, CFRP exhibits non-linear failure [37]. CFRP propellers, especially those with nickel-cobalt leading edges are preferred due to high strength-to-weight ratio[38] and repairability compared to metallic blades [36].

3.7.2 Vibration and balancing

Propellers must follow ISO 21940-11:2016 standard [39], targeting a "G 6.3" balance grade [40]. The Campbell Diagram is the essential tool for visualizing the relationship between natural frequencies and rotational speed, accounting for centrifugal stiffening and avoiding critical resonance "order lines" [41].

3.8 Performance quantification: Dimensionless coefficients and efficiency

Dimensionless analysis allows for the comparison of propellers across varying scales and atmospheric densities [30]. Performance is defined by three primary coefficients:

- Thrust Coefficient:

$$C_T = \frac{T}{\rho n^2 D^4} \quad ...(12)$$

- Power Coefficient:

$$C_P = \frac{P}{\rho n^3 D^5} \quad ...(13)$$

- Torque Coefficient:

$$C_Q = \frac{Q}{\rho\, n^2 D^5} \quad ...(14)$$

The Advance Ratio is given by:

$$J = \frac{V_\infty}{nD} \quad ...(15)$$

J acts as a generalized angle of attack [30].

Propulsive efficiency (η) is formulated as:

$$\eta = \frac{C_T \cdot J}{C_P} \quad ...(16)$$

Fixed-pitch propellers are optimized for a single J, whereas variable-pitch systems offer a broader composite efficiency envelope [42].

3.9 Operational reality

The certification of UAM platforms is heavily dependent on aeroacoustics. Noise is categorized into Tonal Noise (thickness and loading noise at the blade-passing frequency) [43] and Broadband Noise (stochastic noise from turbulence ingestion and blade-wake interaction) [44].

Furthermore, Density Altitude greatly impacts operations. High-elevation or high-temperature conditions simultaneously degrade thrust [45] and reduce the cooling efficiency of electric motors [46]. Mission-specific configurations, such as coaxial rotors, offer compact footprints but typically suffer a 17–29% power penalty due to aerodynamic interference between the disks [47].

4.0 Airfoil Selection for Propeller Design: Parameters and Trade-Offs

4.1 Strategic context of propeller aerodynamics

The design and optimization of a propeller represent a complex interdisciplinary problem, requiring a nuanced synthesis of aerodynamic theory, structural mechanics and aeroacoustics. A single blade often bridges multiple aerodynamic regimes, with varying flow conditions along the blade span [48]. The key challenge is the reconciliation of maximum propulsive efficiency—manifested as thrust generation—with the rigid structural and acoustic constraints inherent in high-velocity rotation [49]. Aerodynamic performance cannot be evaluated in isolation. It must be balanced against the centrifugal loads that scale with the square of the rotational speed and the noise signatures that dictate environmental and operational viability [49].

4.2 Reynolds number variations and boundary layer physics

For a rotating blade, the local Reynolds number varies significantly along the radius because the local velocity (V_{local}) increases significantly toward the tip. This local velocity is defined as:

$$V_{local} = \sqrt{V_{forward}^2 + (\Omega r)^2} \quad ...(17)$$

where $V_{forward}$ is the axial velocity and Ωr represents the rotational velocity at radius r [50].

The following table categorizes optimal airfoil characteristics based on the operational scale and Re sensitivity of the aircraft.

Table 5: Reynolds Number Regimes in Propeller Design

Reynolds Number Regime	Typical Application	Optimal Airfoil Characteristics
Ultra-Low ($Re < 5 \times 10^4$)	Micro-Drones, MAVs	Very thin, high camber, often flat plates to manage separation [33] .
Low (5×10^4 *to* 2×10^5)	Small UAVs, Hobby Drones	Thin airfoils (3-5% thickness), high camber (e.g., Selig S1223) [33], [51].
Moderate (2×10^5 *to* 10^6)	General Aviation, STOL UAVs	Transitioning from high-lift to standard sections (e.g., NACA 4412, E387) [51], [52].
High ($Re > 10^6$)	Turboprops, Transport Aircraft	Specialized high-speed sections for boundary layer stability (e.g., NACA 16-series) [17], [33], [48].

Designers need to account for the hysteresis and unsteady aerodynamic phenomena triggered by fluctuation in Re [33], which can lead to harmful blade vibration [53]. This sensitivity directly influences the efficiency of the propeller system.

Doi: 10.51976/jfsa.722403

4.3 The lift-to-drag ratio and propulsive efficiency metrics

While the L/D ratio is a traditional benchmark for airfoil performance, its contribution to total propeller efficiency must be analyzed through power balance. In axial flight, the total power (P) consumed by the propeller is expressed as:

$$P = T \cdot V + T \cdot v_a + P_{Cd} \quad ...(18)$$

where $T \cdot V$ is propulsive power, $T \cdot v_a$ is induced power [54] and P_{Cd} is the profile drag power [49].

For long-endurance solar-powered UAVs, this profile drag becomes a critical design driver [55]. Airfoil inefficiency increases required current draw, reducing effective battery capacity due to Peukert's effect [56] and consequently amplifying losses and reducing endurance [57]. This gives the need for airfoils that maintain stable performance not only in cruise, but across the range of angles of attack encountered throughout the discharge cycle.

4.4 Stall behavior and operational stability dynamics

Stall characteristics are a vital safety and stability parameter, particularly during high-power maneuvers such as takeoff and climb where local blade sections operate near their maximum lift coefficients ($C_{L,max}$) [58]. The mechanism of separation dictates the mechanical health of the propulsion system. Trailing-edge stall is generally gradual, characterized by a rounded lift curve that results in a predictable reduction in thrust[58] and gentle vibratory feedback [9].

In contrast, leading-edge stall, which is common in thin, high-speed profiles is abrupt and catastrophic. The sudden collapse of flow over the upper surface generates severe impulsive loading and a high-frequency "slap" noise [58]. At high angles of attack, aerodynamic loading between the advancing and retreating blades of the propeller becomes non-linear if the airfoil exhibits abrupt stall [50]. This creates sudden yawing and pitching moments which are difficult to manage by both pilots and flight control systems [50].

4.5 Structural and manufacturing constraints in blade geometry

A propeller blade is a cantilever beam subjected to extreme centrifugal loads [50] and aerodynamic bending moments [9]. These structural realities mandate a significant radial variation in the thickness-to-chord (t/c) ratio. Root sections typically require t/c values of 20% to 25% to provide the internal depth necessary for hub attachment and load transfer [50]. Conversely, tip sections are kept thin (3% to 6%) to mitigate compressibility losses [48] and noise [9].

Table 6: Impact of Material Selection on Airfoil Geometry

Material Class	Thickness/Structural Logic	Aerodynamic Consequence
Wood	Requires ~33% more thickness for stiffness against torsional loads [61].	Higher profile drag and lower efficiency (~3-4% loss vs. metal) [61].
Metal (Aluminum)	Allows for thinner, high L/D sections and higher tip speed limits (~950 fps) [61].	Susceptible to fatigue and surface roughness (nicks) [36], [62].
Composite (Carbon)	Highest strength-to-weight, allows for complex 3D swept geometries [36], [62].	Maintains optimized dimensions, enables complex, thin-tip designs [36], [62].

Manufacturing limitations also drive geometry. In composite structures, a finite trailing edge thickness is required to ensure a strong bond between the upper and lower skins [59]. A sharp edge would lead to high stress concentrations and eventual delamination [49]. Thus, airfoils are often

"truncated" or blunted [60]. Carbon composites represent the modern standard, enabling the realization of complex 3D geometries and swept tips [62] that are impossible with traditional materials [36].

4.6 Comparative review of airfoil families

Table 7: Key Characteristics of Selected Airfoil Families

Airfoil Family	Description / Characteristics
NACA Four-Digit Series (e.g., NACA 4412)	Robust against surface contamination and roughness. Used as a standard for general aviation propellers operating in field conditions. [17], [63]
NACA 6-Series	Provides low drag through laminar flow but is highly surface-sensitive, leading-edge contamination (insects, rain) moves the boundary layer transition point forward, causing the drag bucket to disappear and degrading performance below simpler sections. [17], [63], [64]
Selig and Eppler (UIUC) Families (e.g., S1223, E387)	Optimized for low-Reynolds-number regimes of UAVs S1223 is a high-lift benchmark, while Eppler E387 maintains flow attachment at low speeds, suitable for long-endurance micro-UAVs [51], [52].
NACA 16-Series and ARA-D	Designed for high-speed applications using inverse design theory, shapes are defined to achieve specific pressure distributions that avoid low-pressure peaks [17], [48], [65].

Figure 4: Airfoil Profiles of E387, NACA 4412 and Selig 1223 [1]

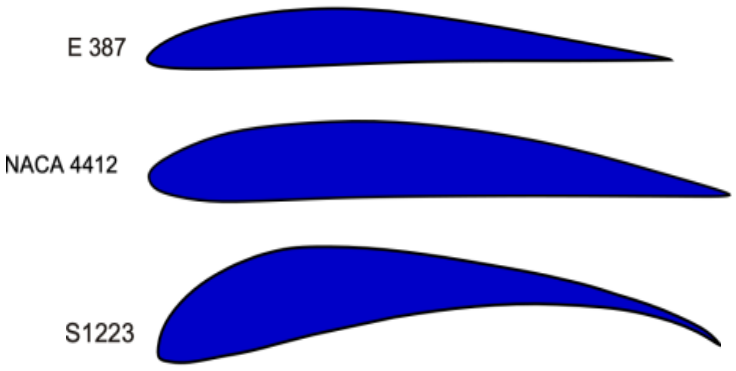


Table 8: Airfoil Model Performance Comparison

Airfoil Model	Max C_L	Stall Angle	Max Thickness	Primary Use Case
Selig S1223	2.36	14.0°	12.1%	High-lift, low-speed UAVs [51].
Eppler E423	2.01	13.5°	12.5%	STOL applications [51].
Eppler E387	~1.4	~12.0°	9.0%	Optimized for attachment at low Re [51], [52].
NACA 4412	~1.6	15.0°	12.0%	General purpose robust props [66].

4.7 Acoustic signatures and environmental impact

Propeller noise is a composite of thickness noise (displaced air volume) [67], loading noise (pressure gradients) and broadband noise (turbulence) [68]. Airfoil selection—specifically the management of peak pressure gradients—is the primary tool for signature mitigation.

Doi: 10.51976/jfsa.722403

Table 9: Acoustic Sources and Airfoil Mitigation Strategies

Acoustic Mechanism	Airfoil Influence	Mitigation Strategy
Loading Noise	Sectional C_L and pressure distribution.	Use thinner airfoils to reduce peak pressure gradients [67].
Thickness Noise	Function of total volume of air displaced.	Reduce t/c ratio at the tips to lower displaced volume [48], [63].
Impulsive "Slap"	Caused by the compact nature of the tip vortex.	Use swept-tip airfoils to diffuse the vortex core [36], [68], [69].
Broadband Noise	Boundary layer turbulence and separation.	Maintain laminar flow (NACA 6-series) to delay transition [64], [66].

Reducing tip Mach numbers via thinner airfoils remains the most effective noise reduction strategy, as tip speeds are the primary driver of thickness and loading noise [62], [67].

4.8 Specialized regimes: Marine cavitation and transonic flow

These principles extend into extreme environments such as marine propulsion, where the primary constraint is cavitation—"cold boiling" where local pressure drops below vapor pressure [70]. While rounded leading edges suffice for slow vessels, moderate speeds utilize ogival or flat-faced sections to distribute pressure more evenly and delay bubble formation [60]. For high-speed applications, "supercavitating" wedge-shaped sections are used to enclose the suction side in a vapor cavity, preventing erosion [60], [70]. In the transonic regime, propeller tips utilize supercritical airfoils like the ARA-D [48]. These sections feature a "flat" upper surface to manage supersonic flow and a "cusped" trailing edge to recover pressure without triggering shock waves [48]. Furthermore, in rotorcraft or high-vibration environments, airfoils with reflexed camber (where the trailing edge curves upward) are used to reduce the pitching moment (C_m) to zero [9], protecting pitch links from fatigue [49] and preventing "stall flutter"—the periodic separation that can destroy powertrains and avionics [53].

5.0 Optimization: Computational and Experimental Approach

5.1 Introduction

The propeller remains the primary energy conversion component in aerospace and marine propulsion, serving as the interface between a power plant's rotational energy and the fluid medium [63]. In modern propulsion systems, optimization is driven by competing aerodynamic, structural and operational constraints. Designers must reconcile disparate regimes, such as the laminar-dominant, low Reynolds number environments of small-scale Unmanned Aerial Vehicles (UAVs) [71] against the shock-dominated transonic tip speeds of high-speed transport aircraft [72]. A key driver of optimization is engine–propeller matching. A propeller's torque absorption characteristics must be meticulously aligned with the prime mover's torque curve [63]. Improper matching can cause "lugging," where the engine operates inefficiently at high load and low RPM, reducing efficiency and increasing wear. Consequently, optimization serves as the mathematical bridge that resolves these multidisciplinary pressures to ensure operational longevity and sustainability.

5.2 Defining the objective function: Mathematical metrics for performance

The prerequisite for any rigorous optimization framework is the definition of a clear objective function—the "North Star" that guides the computational solver. In the absence of a mathematically

articulated goal, designers cannot navigate the trade-offs between thrust, efficiency and environmental impact. In the aerodynamic domain, performance is evaluated using standard non-dimensional coefficients (C_T, C_P and η). While maximizing η is a universal priority, sector-specific objectives vary significantly. In marine propulsion, the objective often centers on minimizing the "cavitation area ratio" to prevent material erosion and acoustic detection [72]. In the Urban Air Mobility (UAM) sector, the objective function is dominated by noise abatement. Using the Ffowcs Williams-Hawkings (FW-H) framework, designers isolate thickness noise (displacement-driven) from loading noise (aerodynamic force-driven) [43] to minimize the perceived sound pressure level (SPL) [44]. These metrics provide the quantitative foundation for the methodologies that follow.

5.3 Computational methodologies

Computational approaches for propeller optimization span multiple fidelity levels. Blade Element Momentum (BEM) theory is widely used for initial design due to its low computational cost and reasonable accuracy [73]. However, it is limited in capturing complex three-dimensional flow interactions and non-uniform inflow conditions encountered in advanced configurations such as eVTOL and Boundary Layer Ingestion systems [74].

Higher-fidelity methods based on Reynolds-Averaged Navier–Stokes (RANS) simulations provide improved accuracy but at significantly higher computational expense. These methods enable detailed analysis of wake interactions, tip vortices and aerodynamic loading [75].

Adjoint-based methods enable efficient gradient computation with respect to a large number of design variables, making them particularly suitable for high-dimensional optimization problems [76]. These approaches generate sensitivity maps that guide localized geometric modifications for rapid convergence [43], [75].

However, high-fidelity gradient-based approaches are not always suitable for highly non-linear or multi-modal design spaces, where gradient information may become unreliable or computationally expensive. This limitation compels the use of alternative optimization strategies, such as heuristic and evolutionary algorithms.

5.4 Heuristic search and evolutionary algorithms

For complex and non-linear design spaces, gradient-free optimization methods are widely used. Genetic Algorithms (GA) and Particle Swarm Optimization (PSO) are commonly applied to explore global optima in propeller design problems [77], [78]. While GA offers robust global exploration through stochastic crossover and mutation [78], PSO often demonstrates faster convergence due to its collective information-sharing mechanism, making it computationally more efficient for continuous optimization problems [78]. These methods are particularly effective in handling multi-variable optimization involving chord, twist and pitch distributions.

To further accelerate optimization, Reduced-Order Models (ROM) and machine learning-based surrogate models are increasingly employed, enabling rapid evaluation of large design spaces with minimal loss in accuracy [72].

5.5 Multidisciplinary design optimization (MDO) and aero-structural trade-offs

In real-world engineering, a propeller cannot be optimized for aerodynamics in isolation. MDO is required to identify the "Utopia Point"—the theoretical limit where conflicting aerodynamic, structural and acoustic objective curves intersect to form a feasible design [79].

Doi: 10.51976/jfsa.722403

The "Aero structural Contradictions" are particularly severe: while high-aspect-ratio, thin airfoils minimize drag, they are structurally vulnerable to centrifugal loads [79], [80]. Engineering data reveals that reducing a blade chord to 50% of its baseline can lead to an 87.5% reduction in bending stiffness and a 75% reduction in bending strength [79]. MDO frameworks resolve these issues by identifying the Pareto-optimal set [79], providing a decision-support tool to balance pairs like Takeoff Distance vs. Horizontal Speed or Noise vs. Power Consumption [81]. Table 10 summarizes the quantitative gains achieved through these integrated MDO strategies:

Table 10: Performance Improvements through Optimization

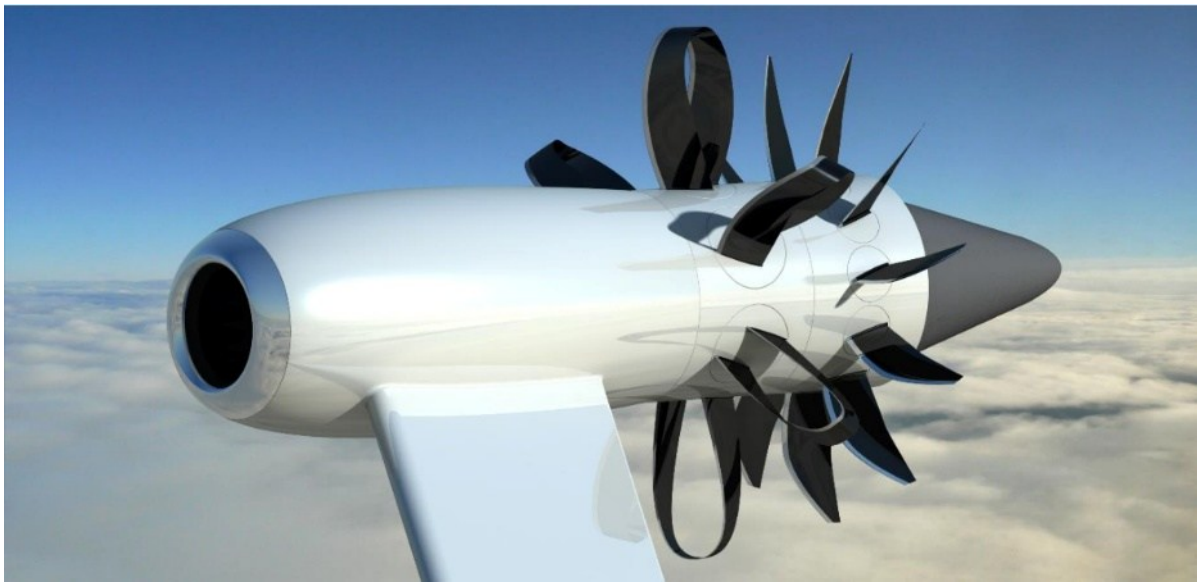
Optimization Target	Base Performance	Optimized Performance	Improvement
Marine Propeller (Thrust)	Baseline Potsdam	Optimized Design	+6% Thrust [72]
Marine Propeller (Efficiency)	Baseline Potsdam	Optimized Design	+3% Efficiency [72]
Marine Propeller (Cavitation)	Baseline Potsdam	Optimized Design	-23.5% Cavitation [72]
UAV Hover Thrust	Original Airfoil	Adjoint-Optimized	+9.46% Thrust [82]
UAM/eVTOL Noise	Modern Baseline	Swept-Blade BEMT	-2.9 dB Noise [83]
Scale Drone Efficiency	Commercial Prop	MATLAB Optimized	+16% Efficiency[71]

These results underscore the impact of rigorous optimization: a 23.5% reduction in cavitation drastically increases component life, while a 16% efficiency gain in drones translates directly to increased mission radius.

5.6 Experimental validation and advanced geometric innovations

Computational models are mathematical predictions that require "A-posteriori verification" through physical testing in wind tunnels or cavitation tanks to ensure consistency with real-world physics [84]. This validation loop has facilitated the rise of non-traditional geometries such as Toroidal propellers[85] and "Boxprops"[86] , demonstrating how experimental validation not only verifies but actively drives geometric innovation.

Figure 5: Air is Flowing from Left to Right, the Front Rotor is Composed of a Boxprop [94]



Boxprops, which use swept blade halves to mitigate interference, have demonstrated a 7% increase in efficiency alongside a 46% reduction in tip vortex strength [86]. The design of such complex shapes relies on advanced parameterization tools like Bezier curves[31] or Free-Form Deformation (FFD) [86]. Furthermore, optimization through variable pitch or refined twist distributions "flattens" the efficiency-advance ratio (J) curve, allowing the vehicle to maintain peak performance across a wider speed envelope rather than being limited to a narrow parabolic peak [87].

6.0 Propeller Integration in Uav and Micro Uav Systems: A Technical Review

6.1 Introduction: The propeller as the primary nexus of UAV design

The propulsion architecture of an Unmanned Aerial Vehicle (UAV) represents the primary nexus where energy storage, power conversion and aerodynamic force generation intersect. In traditional manned aviation, propellers are typically sized to match pre-existing reciprocating or turbine engines. However, the design of modern electric UAVs—and specifically Micro UAVs (MUAVs)—has undergone a strategic shift toward a propeller-centric methodology [88], [89]. The propeller is not merely an individual component but the central one that dictates the operational envelope, structural requirements and electrical architecture of the entire platform [90].

This "top-down" design methodology recognizes that the propeller serves as the first point of interaction between the vehicle and its environment. By establishing the propeller's performance characteristics as the initial step in the design workflow, engineers can rigorously determine the subsequent mechanical loads and electrical demands placed upon the motor, electronic speed controller (ESC) and battery [90].

6.2 Aerodynamic fundamentals and reynolds number sensitivity

Propeller serves as the primary energy conversion device in a UAV system, converting electrical potential into fluid momentum. This conversion defines the hard limits of a system's thrust and endurance [90]. The fundamental equations for Thrust (T) and Power (P) are expressed using standard aerospace coefficients:

$$T = C_T \rho n^2 D^4 \quad ...(19)$$

$$P = C_P \rho n^3 D^5 \quad ...(20)$$

In these equations, ρ represents air density, n is the rotational speed and D is the propeller diameter [89]. These scaling laws highlight strong sensitivity to physical dimensions. A mere 10% increase in diameter results in an approximate 61% increase in power demand [89], requiring a substantial expansion in battery capacity and discharge capability.

Table 11: Comparison of Design Constraints for Large and Micro UAVs

Feature	Large UAV Systems	Micro UAV Systems (MUAV)
Typical Diameter	>15 inches	2 - 9 inches [91], [92]
Reynolds Number (Re)	>200,000	<100,000 [92], [93]
Aerodynamic Sensitivity	Moderate, robust turbulent flow	High. Volatile laminar separation [94], [95]
Efficiency Mismatch	Tolerable within 5-10% margins	Critical. In some cases, may lead to mission failure [92], [94]
Design Focus	Structural integrity and cruise speed	Low-speed lift and noise reduction [95], [96]

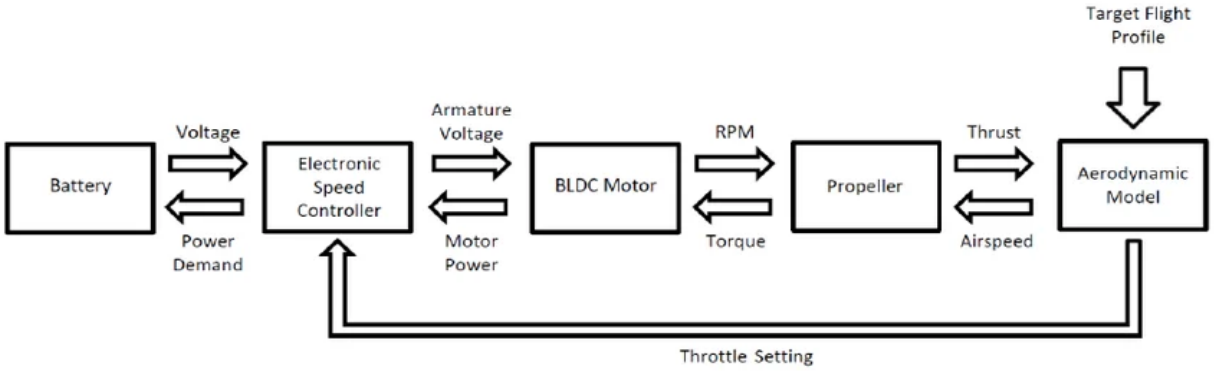
Table 11 contrasts the aerodynamic regimes and design priorities across different UAV scales. This data shows why MUAVs require custom-designed airfoils.

Doi: 10.51976/jfsa.722403

6.3 Mechatronic synergy: Motor-propeller matching and battery sizing

The motor and propeller constitute the "mechanical core" of the propulsion system and their synergy is the most critical factor in ensuring system longevity [88]. Matching the motor's K_v rating (RPM per volt) to the propeller diameter and pitch is essential.

Figure 6: Block Diagram of a Propulsion Model [105]



Low K_v motors, produce high torque for large propellers (10–30 inches) to maximize hover efficiency [91], [97]. Conversely, high K_v motors are paired with smaller props (2–5 inches) for agile flight where rapid RPM changes are prioritized [91], [98].

The "Operating Point" of the system is defined by the intersection of the propeller's load curve—which increases cubically with RPM—and the motor's efficiency curve [88], [99]. If these curves intersect in a low-efficiency zone, significant energy is wasted as heat. In MUAVs, this is particularly hazardous as small motors (e.g., 1103 to 1404 sizes) have very limited thermal mass, making them highly susceptible to damage from over-torque conditions [91], [100]. Furthermore, improper matching can lead to ESC saturation, where the controller reaches 100% duty cycle but the motor cannot reach the required RPM, causing a total loss of control authority [88], [91].

Cruising efficiency is governed by the Advance Ratio(J). High-pitch propellers may offer better cruising speeds but suffer from higher profile drag at zero advance ratio (hovering condition), leading to an increased power consumption [32], [89]. Battery sizing must balance these demands. Moving to higher voltage (e.g., using 6S instead of 4S) minimizes I^2R resistive loss, though it requires more complex ESCs with advanced MOSFETs and robust insulation [100], [101].

Table 12: Engineering Priorities for Power Distribution based on the Specific Phase of Flight

Mission Phase	Propeller Requirement	Battery Sizing Driver
Hovering	High thrust/watt efficiency	Total capacity (mAh) [99], [102]
Cruising	High advance ratio efficiency	Voltage (V) for I^2R minimization [91], [100]
Maneuvering	Low rotational inertia	Peak discharge rate (C) [91], [98]
Heavy Lift	Large diameter/low pitch	Sustainable high-load current [88], [91]

This coupling between aerodynamic loading and electrical performance reinforces the necessity of treating propulsion as an integrated electromechanical system rather than independent subsystems.

6.4 Structural dynamics and aero-elastic constraints

The propeller acts as a source of both static and dynamic loads that dictate the structural integrity of the UAV [103], and three critical loads must be managed. Centrifugal forces, where at high RPM the blades constantly experience massive outward forces requiring the use of high-tensile materials like carbon fiber [103] and robust hub designs [50] to prevent blade ejection from the hub. Vibrational loads, which scale with the square of RPM, where mass imbalances create centripetal forces [104] that lead to structural fatigue in motor arms [105]. Thirdly, gyroscopic effects, where during pitch or yaw motion the angular momentum ($L = I\omega$) results in a gyroscopic precession moment [106] that must be resisted by the frame's torsional stiffness to prevent "frame twist" [107].

Furthermore, engineers must avoid resonance between the "Blade Pass Frequency" ($RPM \times blade\ count$) and the frame's natural frequency. This prevents catastrophic vibration that can loosen fasteners, damage solder joints and disturb MEMS sensors [103], [108].

6.5 Control authority and flight stability

The propeller is the primary actuator for the flight controller (FC). Its responsiveness is limited by rotational inertia (I). Larger, heavier propellers have high moment of inertia. This created a delay between the FC's command and change in propeller speed, which can lead to oscillations in turbulent conditions. To maintain stability, the FC employs "Thrust Linearization" algorithms [109].

6.6 Systemic failure modes of suboptimal propeller selection

Suboptimal selection of propeller triggers a series of cascading failures across the system [88]. Aerodynamic issues, where if the blade section's angle of attack is too high for the operating Reynolds number, flow separates prematurely [92] and operation outside the optimal Re range also causes early stall [94] and excessive pressure drag, draining the battery prematurely [95]. Electrical/thermal issues, where motor overloading can cause overheating, internal shorts, and reduced motor lifespan [91]. High current draw causes battery "voltage sag" [98], which in MUAVs can trigger in-flight FC reboots [99]. Lastly, mechanical/stability issues, where thin nylon blades may undergo "coning" (bending forward under thrust) [50]. This alters the aerodynamic profile and reduces efficiency [99].

7.0 Research Gaps, Limitations and Future Directions

Despite major advances in airfoil theory, propeller aerodynamics, optimization and UAV integration, several key limitations remain across the design pipeline.

At the airfoil level, emerging directions include active flow control and morphing airfoils, enabling adaptive performance across flight regimes. These are especially relevant for extreme environments such as Martian flight, where low Reynolds number and compressibility effects coexist [110]. However, practical implementation is limited by material, actuation and control challenges.

With increasing computational power, Multi-Disciplinary Optimization (MDO) now integrates aerodynamic, structural and acoustic constraints into unified frameworks [10]. Yet, current models still struggle with strongly coupled nonlinear effects, particularly in Low-Reynolds-number and unsteady UAV regimes.

In propeller analysis, Blade Element Momentum Theory (BEMT) still shows limitations in hover [111] and unsteady transition regimes, especially in tilt-rotor systems where asymmetric inflow causes thrust oscillations between advancing and retreating blades [112]. Structural vibration control

also remains critical, requiring Modal Analysis and Campbell diagrams to avoid resonance-induced failure [41]. The field is rapidly shifting toward autonomous design systems, where Deep Reinforcement Learning (DRL) optimizes both blade geometry [77] and flight trajectories for objectives such as urban noise reduction [113]. Coupled with high-fidelity RANS solvers, these methods are expected to push propulsion systems toward near-physical performance limits [80], aided by Reduced-Order Modeling (ROM) for rapid iteration [72].

However, a major unresolved challenge is system-level coupling, where propeller performance is strongly influenced by motor, battery, structural and control system interactions, demanding fully integrated co-design approaches.

At the system level, the industry is moving toward holistic MDO frameworks that unify aerodynamic, structural and electrical constraints [89], [114]. Tools like XFOIL and BEMT are used to identify global optima [94], sometimes revealing counterintuitive solutions such as heavier motors yielding better system efficiency under specific loads [88], [115]. Future trends include bio-inspired and morphing propellers [116], adaptive geometries and flapping-wing concepts for real-time performance tuning [96], [117]. Acoustic optimization via tip-speed control is also becoming essential for urban air mobility.

Overall, UAV propulsion is evolving toward an intelligent, integrated design ecosystem where performance is optimized at the system level rather than at isolated component scales.

8.0 Conclusion

This review presents a mixture of UAV and micro-UAV aerodynamic systems, integrating airfoil theory, propeller aerodynamics, optimization techniques and system-level design. Foundational principles such as lift generation, pressure distribution and Reynolds number effects govern airfoil performance, while Low-Reynolds-number regimes introduce challenges like laminar separation and early stall, highlighting the need of specialized geometries. Propeller analysis extends these concepts into rotating systems, where methods such as momentum theory, Blade Element Theory and BEMT provide predictive capability, further enhanced by CFD-based approaches. Modern optimization frameworks, including evolutionary algorithms and Multi-Disciplinary Design Optimization (MDO), enable systematic trade-off analysis across aerodynamic, structural and acoustic domains. Crucially, propeller performance is inherently coupled with motor characteristics, battery limitations and control dynamics, reinforcing the need for integrated system design. Overall, UAV propulsion is evolving toward a cohesive, computation-driven paradigm that combines physics-based modeling with adaptive optimization to enable efficient, high-performance aerial systems.

References

[1] J. G. Leishman, “Aerodynamics of Airfoil Sections,” Jan. 2023, doi: 10.15394/eaglepub.2022.1066.n23.

[2] Aerodynamic Forces. Accessed: Apr. 06, 2026. [Online]. Available: https://www.grc.nasa.gov/www/k-12/VirtualAero/BottleRocket/airplane/presar.html

[3] “Aerodynamic Lift, Drag and Moment Coefficients,” AeroToolbox. Accessed: Apr. 06, 2026. [Online]. Available: https://aerotoolbox.com/lift-drag-moment-coefficient/

[4] J. G. Leishman, “Aerodynamics of Airfoil Sections,” Jan. 2023, doi: 10.15394/eaglepub.2022.1066.n23.

[5] Cornell University, "Aerodynamic Background." [Online]. Available: https://courses.cit.cornell.edu/mae5070/AeroBackground.pdf

[6] Y. D. Dwivedi, P. Pavithra, E. Parimala, and Y. Meena, "XFOIL analysis on low reynolds number airfoil," *Grad. Res. Eng. Technol.*, pp. 9–17, Apr. 2022, doi: 10.47893/GRET.2022.1082.

[7] H. Shah, S. Mathew, and C. M. Lim, "A Novel Low Reynolds Number Airfoil Design for Small Horizontal Axis Wind Turbines," *Wind Eng.*, vol. 38, no. 4, pp. 377–391, Aug. 2014, doi: 10.1260/0309-524X.38.4.377.

[8] "Pitching moment," *Wikipedia*. Dec. 30, 2024. Accessed: Apr. 06, 2026. [Online]. Available: https://en.wikipedia.org/w/index.php?title=Pitching_moment&oldid=1266189476

[9] J. G. Leishman, "Airfoil Shapes," Jan. 2023, doi: 10.15394/eaglepub.2022.1066.n21.

[10] K. S. Dahl and P. Fuglsang, *Design of the wind turbine airfoil family RISØ-A-XX*. in Risø-R, no. 1024. Roskilde: Risø National Laboratory, 1998.

[11] "Airfoils at low Reynolds Numbers | Fluid Mechanics Research Laboratory | University of Waterloo." Accessed: Apr. 06, 2026. [Online]. Available: https://uwaterloo.ca/fluid-mechanics-research-lab/research/airfoils-low-reynolds-numbers

[12] E. Giacomini and L.-G. Westerberg, "CFD Analysis of Transition Models for Low-Reynolds Number Aerodynamics," *Appl. Sci.*, vol. 15, no. 18, p. 10299, Sep. 2025, doi: 10.3390/app151810299.

[13] P. B. S. Lissaman, "Low-Reynolds-Number Airfoils," *Annu. Rev. Fluid Mech.*, vol. 15, no. 1, pp. 223–239, Jan. 1983, doi: 10.1146/annurev.fl.15.010183.001255.

[14] Ashish Kumar Gupta, P.A. Aswatha Narayana, and G. Ramesh, "Numerical Validation of Low Reynolds Number Airfoil for Uav," *J. Aerosp. Sci. Technol.*, vol. 70, no. 3, pp. 164–174, Aug. 2023, doi: 10.61653/joast.v70i3.2018.402.

[15] J. Md. Madha, Dr.-Ing. J. Niessner, and Dr.-Ing. H. Koch-Gröber, "A Comparative Numerical Aerodynamic Study between SD7032 and NACA0015 Aerofoil as Adjustable RearWing for Formula Student Cars," in *Proceedings of the International Conference on Industrial Engineering and Operations Management*, National Institute of Posts and Telecommunications (INPT), Rabat, Morocco: IEOM Society International, Apr. 2025. doi: 10.46254/AF6.20250151.

[16] S. Adiwidodo and A. H. Wijaya, "Simulation of Effect of Airfoil MH32 with Variation Taper Ratio and Angle of Attack Coefficient Lift and Drag Fixed wing Unmanned Aircraft," *Asian J. Sci. Eng.*, vol. 1, no. 1, p. 23, Jun. 2022, doi: 10.51278/ajse.v1i1.396.

[17] Brian Cantwell, "The NACA Airfoil Series," Stanford University, Stanford, CA, USA, Lecture notes/course material. [Online]. Available: https://web.stanford.edu/~cantwell/AA200_Course _Material/The%20NACA%20airfoil%20series.pdf

[18] Richard Eppler, "SOME NEW AIRFOILS," Universität Stuttgart, Stuttgart, West Germany, Technical report. [Online]. Available: https://files01.core.ac.uk/download/pdf/10339737.pdf

[19] M. Drela, "XFOIL: An Analysis and Design System for Low Reynolds Number Airfoils," in *Low Reynolds Number Aerodynamics*, vol. 54, T. J. Mueller, Ed., Berlin, Heidelberg: Springer Berlin Heidelberg, 1989, pp. 1–12. doi: 10.1007/978-3-642-84010-4_1.

[20] M. Drela, "Low-Reynolds-number airfoil design for the M.I.T. Daedalus prototype- A case study," *J. Aircr.*, vol. 25, no. 8, pp. 724–732, Aug. 1988, doi: 10.2514/3.45650.

[21] S. M. Group, "Ubiquitous Supercritical Wing Design Cuts Billions in Fuel Costs." Accessed: Apr. 21, 2026. [Online]. Available: https://www.techbriefs.com/component/content/article/32671-ubiquitous-supercritical-wing-design-cuts-billions-in-fuel-costs

[22] U. Mamadaminov, "Review of Airfoil Structure for Wind Turbine Blades," Sep. 2013.

[23] Robert T. Jones, "Classical Aerodynamic Theory," National Aeronautics and Space Administration (NASA), Ames Research Center, Moffett Field, California, USA, Dec. 1979. [Online]. Available: https://ntrs.nasa.gov/api/citations/19800006774/downloads/19800006774.pdf

[24] Lawrence J. Bober, "Advanced Propeller Aerodynamic Analyses," National Aeronautics and Space Administration Lewis Reasarch Center. [Online]. Available: https://ntrs.nasa.gov/api/citations/19800013858/downloads/19800013858.pdf

[25] "Propeller Performance: An introduction, by EPI Inc." Accessed: Apr. 10, 2026. [Online]. Available: https://www.epi-eng.com/propeller_technology/selecting_a_propeller.htm

[26] Blade element momentum theory. *Wikipedia*. Feb. 13, 2026. Accessed: Apr. 10, 2026. [Online]. Available: https://en.wikipedia.org/w/index.php?title=Blade_element_momentum_theory&oldid=1338171259

[27] M. Tai, W. Lee, D. Kim, and D. Park, "Improvements in Robustness and Versatility of Blade Element Momentum Theory for UAM/AAM Applications," *Aerospace*, vol. 12, no. 8, p. 728, Aug. 2025, doi: 10.3390/aerospace12080728.

[28] S. Gudmundsson, "The Anatomy of the Propeller," in *General Aviation Aircraft Design*, Elsevier, 2014, pp. 581–659. doi: 10.1016/B978-0-12-397308-5.00014-3.

[29] M. F. Hasnaoui, A. Bouhelal, and A. Smaili, "Aerodynamic analysis of a small-scale drone propeller using the blade element momentum method", doi: https://doi.org/10.57056/ajet.v8i2.149.

[30] "PROPELLERS," Universidad Politécnica de Madrid (UPM), Madrid, Spain. [Online]. Available: http://imartinez.etsiae.upm.es/~isidoro/bk3/c17/Propellers.pdf

[31] A. Sedelnikov *et al.*, "Algorithm for Propeller Optimization Based on Differential Evolution," *Computation*, vol. 12, no. 3, p. 52, Mar. 2024, doi: 10.3390/computation12030052.

[32] N. Ismail, N. L. Mohd Kamal, N. Norhashim, S. Abdul Hamid, Z. Sahwee, and S. Ahmad Shah, "Electric Propulsion and Hybrid Energy Systems for Solar-Powered UAVs: Recent Advances and Challenges," *Drones*, vol. 9, no. 12, p. 846, Dec. 2025, doi: 10.3390/drones9120846.

[33] J. Winslow, H. Otsuka, B. Govindarajan, and I. Chopra, "Basic Understanding of Airfoil Characteristics at Low Reynolds Numbers (104–105)," *J. Aircr.*, vol. 55, no. 3, pp. 1050–1061, May 2018, doi: 10.2514/1.C034415.

[34] R. Gopalakrishnan, N. R. R. Ramakrishnan, B. P. R. Dennis, and A. S. L. Kuzhanthai, "Performance Study and Analysis of an UAV Airfoil at Low Reynolds Number," in *Intelligent Manufacturing and Energy Sustainability*, vol. 265, A. N. R. Reddy, D. Marla, M. N. Favorskaya, and S. C. Satapathy, Eds., in Smart Innovation, Systems and Technologies, vol. 265. , Singapore: Springer Singapore, 2022, pp. 107–113. doi: 10.1007/978-981-16-6482-3_11.

[35] "Clark-Y Airfoil Performance at Low Reynolds Numbers," IIHR—Hydroscience and Engineering, University of Iowa, 1984. [Online]. Available: https://stern.lab.uiowa.edu/sites/stern.lab.uiowa.edu/files/2024-11/clark-y-paper.pdf

[36] "Durability, performance define new generation of propellers." Accessed: Apr. 11, 2026. [Online]. Available: https://www.aopa.org/news-and-media/all-news/2025/august/22/hartzell-propeller

[37] M. Kaminski, F. Laurin, J.-F. Maire, C. Rakotoarisoa, and E. Hemon, "Fatigue damage modeling of composite structures: the Onera viewpoint," *AerospaceLab J.*, vol. Issue 9, p. 12 pages, 2015, doi: 10.12762/2015.AL09-06.

[38] K. Patton, "What Are the Benefits of Composite Propellers?," Hartzell Propeller. Accessed: Apr. 10, 2026. [Online]. Available: https://hartzellprop.com/benefits-of-composite-propellers/

[39] "Drone Propeller Balancing Techniques & Standards," Unmanned Systems Technology. Accessed: Apr. 11, 2026. [Online]. Available: https://www.unmannedsystemstechnology.com/feature/drone-propeller-balancing-techniques-standards/

[40] "Two Methods for Balancing Drone Propellers to Boost UAV Performance," Unmanned Systems Technology. Accessed: Apr. 11, 2026. [Online]. Available: https://www.unmannedsystemstechnology.com/feature/two-methods-for-balancing-drone-propellers-to-boost-uav-perform ance/

[41] N. L. Oliveira, A. C. D. C. Lemonge, P. H. Hallak, K. Kyprianidis, S. Vouros, and M. A. Rendón, "Propeller Design Optimization and an Evaluation of Variable Rotational Speed Flight Operation Under Structural Vibration Constraints," *Machines*, vol. 13, no. 6, p. 490, Jun. 2025, doi: 10.3390/machines13060490.

[42] O. Gur, "Maximum Propeller Efficiency Estimation," *J. Aircr.*, vol. 51, no. 6, pp. 2035–2038, Nov. 2014, doi: 10.2514/1.C032557.

[43] L. Abergo, B. Y. Zhou, and A. Guardone, "Tonal noise optimization of propeller using a steady adjoint method," *J. Acoust. Soc. Am.*, vol. 158, no. 1, pp. 651–662, Jul. 2025, doi: 10.1121/10.0037217.

[44] J. Hua and R. R. Mankbadi, "Prediction and Control of Broadband Noise Associated with Advanced Air Mobility—A Review," *Appl. Sci.*, vol. 14, no. 18, p. 8455, Sep. 2024, doi: 10.3390/app14188455.

[45] A. Faishal, I. T. Setyadewi, N. Aklis, F. Harjanto, A. M. Wibowo, and A. Supriyanto, "Comparative Study of Propeller Thrust Force on Unmanned Aerial Vehicle Using Ground Testing Methods and Theoretical Calculations," in *The 8th Mechanical Engineering, Science and Technology International Conference*, MDPI, Feb. 2025, p. 59. doi: 10.3390/engproc 2025084059.

[46] K. Patton, "How Does Density Altitude Affect Flight?," Hartzell Propeller. Accessed: Apr. 11, 2026. [Online]. Available: https://hartzellprop.com/how-does-density-altitude-affect-flight/

[47] W. Ong, S. Srigrarom, and H. Hesse, "Design Methodology for Heavy-Lift Unmanned Aerial Vehicles with Coaxial Rotors," in *AIAA Scitech 2019 Forum*, San Diego, California: American Institute of Aeronautics and Astronautics, Jan. 2019. doi: 10.2514/6.2019-2095.

[48] A. J. Bocci, "A New Series of Aerofoil Sections Suitable for Aircraft Propellers," *Aeronaut. Q.*, vol. 28, no. 1, pp. 59–73, Feb. 1977, doi: 10.1017/S0001925900007939.

[49] O. Gur, "Does Propeller Performance Depend on Airfoil Design?".

[50] "Aviation Maintenance Technician Handbook—Powerplant (FAA-H-8083-32B), Chapter 7: Propellers," Federal Aviation Administration (FAA), U.S. Department of Transportation, 2023. [Online]. Available: https://www.faa.gov/sites/faa.gov/files/09_amtp_ch7.pdf

[51] S. Reza and Samsul Arfin Mahmood, "Performance Analysis And Comparison Of High Lift Airfoil For Low-Speed Unmanned Aerial Vehicle," Dec. 2016, doi: 10.5281/ZENODO.1468120.

[52] T. A. Shams, S. I. A. Shah, A. Javed, and S. H. R. Hamdani, "Airfoil Selection Procedure, Wind Tunnel Experimentation and Implementation of 6DOF Modeling on a Flying Wing Micro Aerial Vehicle," *Micromachines*, vol. 11, no. 6, p. 553, May 2020, doi: 10.3390/mi11060553.

[53] N. D. Khairnar, Dr. A. D. Bagul, and Dr. S. P. Shekhawat, "'An Analysis Of Effect Of Variation In Reynolds Number On Aerodynamic Damping Of Aerofoil Blade With Feasibility Of Active Damping Method,'" *Nanotechnol. Percept.*, vol. 20, no. 7, pp. 4715–4727, Dec. 2024, doi: 10.62441/nano-ntp.v20i7.5472.

[54] R. Octonius and N. Ruseno, "Endurance estimation in hovering flight based on battery power requested on quadcopter UAV," *Angkasa J. Ilm. Bid. Teknol.*, vol. 14, no. 2, Nov. 2022, doi: 10.28989/angkasa.v14i2.1226.

[55] J. Narimanov, "Simulation Analysis of Airfoil for Solar-Powered UAV Applications," *Acad. Open*, vol. 10, no. 1, Mar. 2025, doi: 10.21070/acopen.10.2025.10782.

[56] L. W. Traub, "Range and Endurance Estimates for Battery-Powered Aircraft," *J. Aircr.*, vol. 48, no. 2, pp. 703–707, Mar. 2011, doi: 10.2514/1.C031027.

[57] Y. Xia, R. A. Adjei, S. Ijaz, Y. Zhang, and Y. Shi, "Optimal Endurance Prediction for a Battery-Powered Unmanned Aerial Vehicle with High Aspect Ratio Wings," in *2024 10th Asia Conference on Mechanical Engineering and Aerospace Engineering (MEAE)*, Taichang, China: IEEE, Oct. 2024, pp. 1761–1769. doi: 10.1109/MEAE62008.2024.11026518.

[58] J. G. Leishman, "Stalling & Spinning," Jan. 2023, doi: 10.15394/eaglepub.2022.1066.n41.

[59] "aircraft design - Why are the trailing edges of wings not always made as 'sharp' as possible?," Aviation Stack Exchange. Accessed: Apr. 11, 2026. [Online]. Available: https://aviation.stackexchange.com/questions/97367/why-are-the-trailing-edges-of-wings-not-always-made-as-sharp -as-possible

[60] S. Srivastava, "Numerical Simulations of Supercavitating Propellers and Hydrofoils".

[61] B. Cassidy, "Wood vs. Metal Fixed Pitch Propellers".

[62] "Composite MT Propeller," McFarlane Aviation. Accessed: Apr. 11, 2026. [Online]. Available: http://www.mcfarlaneaviation.com/articles/mt-propeller-composite-propellers/

[63] S. Adebimpe, "Propeller Aerodynamic Design and Optimization," Oct. 2023, doi: 10.20944/preprints202310.0418.v1.

[64] "NACA 6 SERIES Explorer - Academy Innova World." Accessed: Apr. 11, 2026. [Online]. Available: https://www.academyinnovaworld.org/blogs/post/naca6series

[65] Lindsey, W. F., Stevenson, D. B., and Daley, Bernard N., "Aerodynamic Characteristics of 24 NACA 16-Series Airfoils at Mach Numbers Between 0.3 and 0.8," 1948, [Online]. Available: https://ntrs.nasa.gov/citations/19930082349

[66] J. F. M. Iii, "Appendix A: Airfoil Data," Aug. 2021, Accessed: Apr. 11, 2026. [Online]. Available: https://pressbooks.lib.vt.edu/aerodynamics/back-matter/airfoil-data/

[67] C. F. Wisniewski, A. R. Byerley, W. Heiser, K. W. Van Treuren, and T. Liller, "The Influence of Airfoil Shape, Reynolds Number and Chord Length on Small Propeller Performance and Noise," in *33rd AIAA Applied Aerodynamics Conference*, Dallas, TX: American Institute of Aeronautics and Astronautics, Jun. 2015. doi: 10.2514/6.2015-2266.

[68] D. J. Moreau and C. J. Doolan, "An experimental study of airfoil tip vortex formation noise," 2016.

[69] J. G. Leishman, "Aircraft Propellers," Jan. 2023, Accessed: Apr. 11, 2026. [Online]. https://eaglepubs.erau.edu/introductiontoaerospaceflightvehicles/chapter/propellers/

[70] A. Capone, F. Alves Pereira, and F. Di Felice, "Flow and Cavity Measurements in a Super-Cavitating Propeller," *J. Mar. Sci. Eng.*, vol. 12, no. 2, p. 243, Jan. 2024, doi: 10.3390/jmse12020243.

[71] S. D. Prior and D. Newman-Sanders, "Advanced Scale-Propeller Design Using a MATLAB Optimization Code," *Appl. Sci.*, vol. 14, no. 14, p. 6296, Jul. 2024, doi: 10.3390/app14146296.

[72] "Streamlining propeller design with ROM-based optimization." Accessed: Apr. 12, 2026. [Online]. Available: https://engineering.esteco.com/blog/propeller-design-with-rom-based-optimization/

[73] A. Ning. Using blade element momentum methods with gradient-based design optimization," *Struct. Multidiscip. Optim.*, vol. 64, no. 2, pp. 991–1014, Aug. 2021, doi: 10.1007/s00158-021-02883-6.

[74] C. Patrao, "Implementation of Blade Element Momentum/Vortex Methods for the Design of Aero Engine Propellers".

[75] "Aerodynamic shape optimization MDO Lab." Accessed: Apr. 12, 2026. [Online]. Available: https://mdolab.engin.umich.edu/wiki/aerodynamic-shape-optimization.html

[76] S. Batay *et al.*, "Adjoint-Based High-Fidelity Concurrent Aerodynamic Design Optimization of Wind Turbine," *Fluids*, vol. 8, no. 3, p. 85, Feb. 2023, doi: 10.3390/fluids8030085.

[77] I. Gypa, M. Jansson, K. Wolff, and R. Bensow, "Propeller optimization by interactive genetic algorithms and machine learning," *Ship Technol. Res.*, vol. 70, no. 1, pp. 56–71, Jan. 2023, doi: 10.1080/09377255.2021.1973264.

[78] R. Hassan, B. Cohanim, O. De Weck, and G. Venter, "A Comparison of Particle Swarm Optimization and the Genetic Algorithm," in *46th AIAA/ASME/ASCE/AHS/ASC Structures, Structural Dynamics and Materials Conference*, Austin, Texas: American Institute of Aeronautics and Astronautics, Apr. 2005. doi: 10.2514/6.2005-1897.

[79] S. Slavik, J. Klesa, and J. Brabec, "Propeller Selection by Means of Pareto-Optimal Sets Applied to Flight Performance," *Aerospace*, vol. 7, no. 3, p. 21, Mar. 2020, doi: 10.3390/aerospace7030021.

[80] S. A. Zoppelt, H. Koyuncuoglu, and P. He, "High-fidelity Aerostructural Optimization Benchmark for Aircraft Propellers in Hover," in *AIAA SCITECH 2024 Forum*, Orlando, FL: American Institute of Aeronautics and Astronautics, Jan. 2024. doi: 10.2514/6.2024-2773.

[81] O. Gur, J. Silver, R. Dítě, and R. Sundhar, "PROPELLER OPTIMIZATION - STRIVE TO PERFORMANCE / ACOUSTIC TRADE-OFF," in *14th International Conference on Evolutionary and Deterministic Methods for Design, Optimization and Control*, Athens, Greece: Institute of Structural Analysis and Antiseismic Research National Technical University of Athens, 2021, pp. 143–154. doi: 10.7712/140121.7957.18315.

[82] H. Wang, Y. Liao, M. Shen, S. Zhou, and G. Xu, "Numerical Simulation Study on Adjoint-Based Optimization of a Propeller Using Reverse Engineering," *IEEE Access*, vol. 13, pp. 90932–90944, 2025, doi: 10.1109/ACCESS.2025.3572180.

[83] X. Geng, T. Hu, P. Liu, T. Sinnige, and G. Eitelberg, "Analysis of thrust-scaled acoustic emissions of aircraft propellers and their dependence on propulsive efficiency".

[84] Z. Zhang, Y. Zhang, J. Yu, P. Du, and J. Zhao, "Variable Pitch Propeller: Multi-Objective Optimization Design and Performance Analysis," in *2nd International Conference on Green Aviation (ICGA 2024)*, MDPI, Feb. 2025, p. 36. doi: 10.3390/engproc2024080036.

[85] O. Ciftci and S. Cadirci, "Multi-Objective Optimization for Performance Enhancement of a Toroidal Propeller Using CFD and FSI," in *Volume 8: Fluids Engineering*, Portland, Oregon, USA: American Society of Mechanical Engineers, Nov. 2024, p. V008T10A018. doi: 10.1115/IMECE2024-144395.

[86] A. C. Patrao, T. Grönstedt, A. Lundbladh, and G. M. Villar, "Wake Analysis of an Aerodynamically Optimized Boxprop High-Speed Propeller," *J. Turbomach.*, vol. 141, no. 9, p. 091011, Sep. 2019, doi: 10.1115/1.4043974.

[87] A. C. Patrao, "On the Aerodynamic Design of the Boxprop," 2018, doi: 10.13140/RG.2.2.22991.74408.

[88] "UAV Propulsion System: How to Match Motors, ESCs & Propellers," T-MOTOR. Accessed: Apr. 14, 2026. [Online]. Available: https://shop.tmotor.com/blog/uav-propulsion-system-motor-esc-propeller-matching

[89] F. Pollet, S. Delbecq, M. Budinger, and J.-M. Moschetta, "DESIGN OPTIMIZATION OF MULTIROTOR DRONES IN FORWARD FLIGHT".

[90] S. Ileanaju Ugbane, C. Umeaku, I. Peter Idoko, L. Anebi Enyejo, C. Idongesit Michael, and F. Efe, "Optimization of Quadcopter Propeller Aerodynamics Using Blade Element and Vortex Theory," *Int. J. Innov. Sci. Res. Technol. IJISRT*, pp. 1708–1756, Nov. 2024, doi: 10.38124/ijisrt/IJISRT24OCT1820.

[91] "Drone Propulsion Matching Guide: Motors, Props, ESCs & Batteries," LIGPOWER. Accessed: Apr. 14, 2026. [Online]. Available: https://www.ligpower.com/blog/drone-propulsion-matching.html

[92] R. W. Deters, G. K. Ananda Krishnan, and M. S. Selig, "Reynolds Number Effects on the Performance of Small-Scale Propellers," in *32nd AIAA Applied Aerodynamics Conference*, Atlanta, GA: American Institute of Aeronautics and Astronautics, Jun. 2014. doi: 10.2514/6.20 14-2151.

[93] W. A. Jordan, S. Narsipur, and R. Deters, "Aerodynamic and Aeroacoustic Performance of Small UAV Propellers in Static Conditions," in *AIAA AVIATION 2020 FORUM*, VIRTUAL EVENT: American Institute of Aeronautics and Astronautics, Jun. 2020. doi: 10.2514/6.2020-2595.

[94] M. Crona, S. Dinger, P. Samuelsson, H. Strömfeldt, and I. Jonsson, "Low-speed propeller for uav applications, from design to experimental evaluation".

[95] Y. Yao, D. Ma, L. Zhang, X. Yang, and Y. Yu, "Aerodynamic Optimization and Analysis of Low Reynolds Number Propeller with Gurney Flap for Ultra-High-Altitude Unmanned Aerial Vehicle," *Appl. Sci.*, vol. 12, no. 6, p. 3195, Mar. 2022, doi: 10.3390/app12063195.

[96] "Low Noise Propeller for UAV." Accessed: Apr. 14, 2026. [Online]. Available: https://xray.greyb.com/drones/low-noise-propeller

[97] T. Robotics, "How to Calculate Motor Kv & Motor Poles," Tyto Robotics. Accessed: Apr. 14, 2026. [Online]. Available: https://www.tytorobotics.com/blogs/articles/how-to-calculate-motor-poles-and-brushless-motor-kv

[98] "FPV Motors KV Rating Explained:What It Means & How to Choose," LIGPOWER. Accessed: Apr. 14, 2026. [Online]. Available: https://www.ligpower.com/blog/what-is-kv-rating-in-fpv-motors.html

[99] A. Gong and D. Verstraete, "Development of a dynamic propulsion model for electric UAVs," 2015.

[100] xcesc6681, "High Voltage ESCs vs Low Voltage ESCs for Drone Applications - XC-ESC." Accessed: Apr. 14, 2026. [Online]. Available: https://www.xc-esc.com/high-vs-low-voltage-esc-for-drone/

[101] "Electronic Speed Controllers – Military Drone ESC," Defense Advancement. Accessed: Apr. 14, 2026. [Online]. Available: https://www.defenseadvancement.com/suppliers/electronic-speed-controllers-military-drones/

[102] "UAV Propulsion Systems: Maximizing Efficiency for Uncrewed Systems," ePropelled. Accessed: Apr. 14, 2026. [Online]. Available: https://epropelled.com/blogs/blog/uav-propulsion-systems-maximizing-efficiency-for-uncrewed-systems

[103] Dhinnesh S, Guru Prasath K S, and Venkatesh N, "Design and Analysis of UAV Propeller for Composite Materials," *Int. Res. J. Adv. Eng. Hub IRJAEH*, vol. 2, no. 01, pp. 20–26, Jan. 2024, doi: 10.47392/IRJAEH.2024.0004.i1.

[104] T. Robotics, "Vibration in Drones from Imbalanced Propellers," Tyto Robotics. Accessed: Apr. 15, 2026. [Online]. Available: https://www.tytorobotics.com/blogs/articles/vibration-drones-imbalanced-propellers

[105] "How Imbalanced Propellers Cause UAV Vibration," Unmanned Systems Technology. Accessed: Apr. 15, 2026. [Online]. Available: https://www.unmannedsystemstechnology.com/feature/how-imbalanced-propellers-cause-uav-vibration/

[106] B. Wainfan, "Prop Gyro." Accessed: Apr. 15, 2026. [Online]. Available: https://www.kitplanes.com/wind-tunnel-57/

[107] "Gyroscopic Behaviour of Propellers." Accessed: Apr. 15, 2026. [Online]. Available: https://www.supercoolprops.com/articles/gyrovibes.php

[108] "The Impact of Propeller Imbalance on UAV Flight," Defense Advancement. Accessed: Apr. 15, 2026. [Online]. Available: https://www.defenseadvancement.com/feature/the-impact-of-propeller-imbalance-on-uav-flight/

[109] "How Drone Propellers Affect Flight Stability," Potensic. Accessed: Apr. 14, 2026. [Online]. Available: https://store.potensic.com/blogs/news/how-drone-propellers-affect-flight-stability

[110] M. Drela, "Transonic low-Reynolds number airfoils," *J. Aircr.*, vol. 29, no. 6, pp. 1106–1113, Nov. 1992, doi: 10.2514/3.46292.

[111] D. Ingraham, J. S. Gray, and L. V. Lopes, "Gradient-Based Propeller Optimization with Acoustic Constraints," in *AIAA Scitech 2019 Forum*, San Diego, California: American Institute of Aeronautics and Astronautics, Jan. 2019. doi: 10.2514/6.2019-1219.

[112] A. Zanotti, A. Velo, C. Pepe, A. Savino, D. Grassi, and L. Riccobene, "Aerodynamic interaction between tandem propellers in eVTOL transition flight configurations," *Aerosp. Sci. Technol.*, vol. 147, p. 109017, Apr. 2024, doi: 10.1016/j.ast.2024.109017.

[113] Y. Kim, J. Ko, K. Yu, and S. Lee, "Low-noise trajectory optimization of urban air mobility in the urban environment using deep reinforcement learning," *J. Acoust. Soc. Am.*, vol. 158, no. 1, pp. 476–494, Jul. 2025, doi: 10.1121/10.0037186.

[114] M. N M, "Aerodynamic Optimization of UAV'S for Increased Endurance," *Int. J. Res. Appl. Sci. Eng. Technol.*, vol. 13, no. 11, pp. 1248–1256, Nov. 2025, doi: 10.22214/ijraset.2025.75306.

[115] T. Robotics, “Comparing UAV Power System Architectures,” Tyto Robotics. Accessed: Apr. 15, 2026. [Online]. Available: https://www.tytorobotics.com/blogs/customer-stories/analysis-and-modeling-of-uav-power-system-architectures

[116] R. S. Geronel and D. D. Bueno, “An overview on bio-inspired UAVs: State-of-the art, challenges and opportunities,” *Proc. Inst. Mech. Eng. Part G J. Aerosp. Eng.*, vol. 239, no. 12, pp. 1293–1308, Sep. 2025, doi: 10.1177/09544100251329987.

[117] D. Skrna, “Combined propeller blade geometrical modifications to reduce noise emissions of urban air mobility vehicles”.